

Integration of ZnO Microcrystals with Tailored Dimensions Forming Light Emitting Diodes and UV Photovoltaic Cells

Jesse J. Cole, Xinyu Wang, Robert J. Knuesel, and Heiko O. Jacobs*

University of Minnesota, Electrical Engineering Room 4-178, 200 Union Street SE, Minneapolis, Minnesota 55455

Received February 18, 2008; Revised Manuscript Received March 31, 2008

ABSTRACT

This article reports a new integration approach to produce arrays of ZnO microcrystals for optoelectronic and photovoltaic applications. Demonstrated applications are n-ZnO/p-GaN heterojunction LEDs and photovoltaic cells. The integration process uses an oxygen plasma treatment in combination with a photoresist pattern on magnesium doped GaN substrates to define a narrow sub-100 nm width nucleation region. Nucleation is followed by lateral epitaxial overgrowth producing single crystal disks of ZnO with desired size over 2 in. wafers. The process provides control over the dimensions (<1% STD) and the location (0.7% STD pitch variation) of the ZnO crystals. The quality of the patterned ZnO is high; the commonly observed defect related emission in the electroluminescence spectra is completely suppressed, and a single near-band-edge UV peak is observed.

ZnO is a promising material for exciton-based opto-electronic devices including light emitting (LED) and laser diodes because of its direct band gap of 3.3 eV at room temperature and a large exciton binding energy of 60 meV.¹⁻³ Fabrication of LEDs based on ZnO homojunctions, however, has been challenging because of the lag of high quality p-doped ZnO. As a consequence there have been a number of reports on n-ZnO/p-GaN heterojunction LEDs. Most recent work has replaced the polycrystalline ZnO thin films^{1,4-6} with ZnO nanowires^{2,7,8} to potentially benefit from the advantage of the nanowire properties, high crystallinity and fewer grain boundaries. Both forward⁸ and reverse bias⁷ electroluminescence (EL) was reported. The reverse bias emission was attributed to tunneling breakdown where hot carrier injection and recombination predominantly occurred in the GaN film.³ Most of the previous devices including our own,³ however, suffered from defect related emission around 585 nm under the desired forward bias operation. Integration of uniform arrays with control over the dimension and location of the single crystal nanowires has been another challenge that will have to be addressed to produce uniform devices over large areas. A wet chemical approach is desired for reasons of processing cost when compared with gas-phase methods, and a number of patterned and seeded growth methods have been reported. Patterned self-assembled monolayers with hydrophobic and hydrophilic endgroups have been used on silver⁹

or silicon substrates¹⁰ yielding densely packed 400 nm diameter and 2 μm long ZnO nanorods in regions that were 2 μm wide with empty areas in between. Out-of-plane orientation varied but has been improved by seeding ZnO nanocrystals through thermal oxidation of zinc acetate.¹¹ Perfect vertical orientation, however, requires substrates such as GaN, MgAl₂O₄,¹² or sapphire¹³ which can be partially masked with photoresist to achieve patterned growth. Qualitatively, all of these methods produced nanorods in the seeded or unmasked areas with limited control over the location and density on a single component basis. Dense films under continued growth eventually lead to coalescence into a polycrystalline film as the diameter increases with grain boundaries and defects in between. Attempts to reduce the defects have been made. The most successful approach used continued growth in combination with photoresist which can lead to a lateral overgrowth, a previously reported concept to produce high quality GaN thin films;¹⁴ for ZnO on MgAl₂O₄, lateral growth over patterned photoresist improved the dislocation density by a factor of 100 compared with the window region containing coalesced nanorods.¹² Subsequent growth using a second window yielded continuous ZnO thin films with reduced dislocations.¹³

This paper reports the growth of single crystals ZnO with control over the dimensions (<1% STD) and location (0.7% STD pitch variation) yielding n-ZnO/p-GaN heterojunction arrays with uniform geometrical and optical properties. The

* Corresponding author. E-mail: hjacobs@umn.edu.

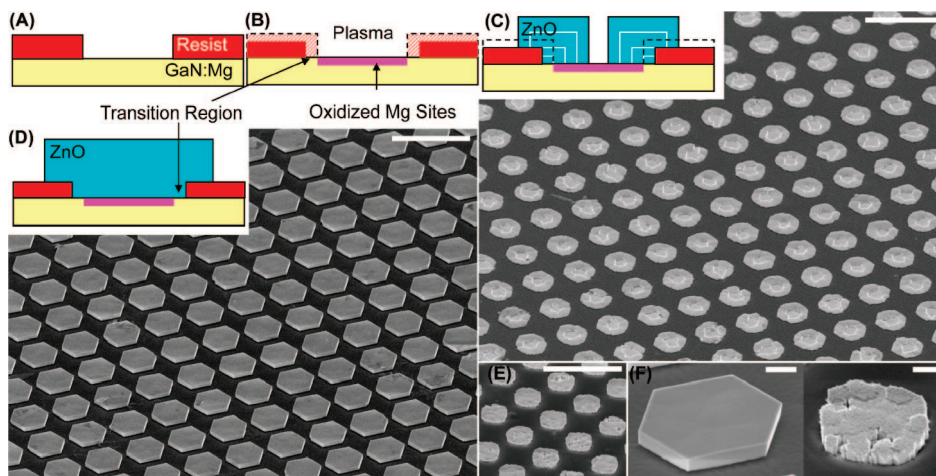


Figure 1. Procedure and results of controlled ZnO microcrystal nucleation and growth involving oxygen plasma treatment. (A) Conventionally patterned photoresist on Mg-doped GaN is exposed to (B) an oxygen plasma to deactivate Mg dopants that otherwise act as nucleation sites. The process produces a transitional region which contains nonoxidized Mg to nucleate growth. Solution growth forms rings (C) that merged into well defined continuous ZnO microcrystals under continuous growth (D). Control experiments without oxygen plasma treatment (E) yield polycrystalline ZnO with grain boundaries and pinhole defects. High magnification SEM images shows a side-by-side comparison of topology difference between plasma-treated (F left) and control samples (F right). 10 μm scale bars in A–E; 1 μm scale bars in F. SEM images taken at 45° tilt.

process uses an oxygen plasma to surface engineer nucleation areas to produce single crystal ZnO disk type structures on p-type GaN at addressable locations on a surface with tailored > 100 nm lateral dimensions and sub-100 nm lateral positional accuracy. The concept uses a plasma process and photoresist patterns to reveal nonoxidized magnesium sites that nucleate growth during hydrothermal growth at 90 °C. Nucleation in nonoxidized areas is followed by epitaxial overgrowth producing patterned areas of ZnO over 2 in. wafers. ZnO/GaN micro-LEDs and UV photovoltaic cells were fabricated. The LEDs possessed strong near band edge electroluminescent emission. Deep-level defect emission in the red and yellow is absent which implies that the ZnO microcrystals are of high quality. A hexagonal star like radiation pattern is observed which is explained by light emission through crystallographic facets.

Figure 1 shows the patterned growth process and the resulting ZnO crystals. Photolithography, oxygen plasma treatment, and solution-based growth are the basic process steps to produce ZnO crystals at exact locations on a surface. The patterned surface (Figure 1A) is formed on a Mg-doped GaN substrate, doping concentration $5 \times 10^{18} \text{ cm}^{-3}$, TDI Inc., Silver Spring, MD. Following a prebake at 115 °C for 60 s, Shipley 1805 photoresist was spun at 3000 rpm, soft-baked at 105 °C for 60 s, exposed using a Karl Suss MA-6 Mask Aligner, and developed in Microposit 351 developer for 30 s. The patterns can directly be used for growth leading to a polycrystalline ZnO film in the exposed GaN areas which shows that the basic developer containing sodium hydroxide and exposure to photoresist do not adversely affect ZnO nucleation on p-type GaN. However, to transition from polycrystalline to the illustrated single crystal structures, plasma treatment was found to be the key (Figure 1B). The treatment yields a nucleation region (Figure 1C inset) at the GaN/photoresist interface. ZnO deposited initially in the ring-shaped regions (Figure 1C), then merged by lateral over-

growth over a longer growth time of 3 h to become the well-faceted hexagonal crystals (Figure 1D). The current understanding of the process involves the Mg dopant, which is the least electronegative atom within the GaN matrix. Nonoxidized Mg is expected to have an affinity to OH^- which reacts with Zn^{2+} to form ZnO during hydrothermal growth. The oxygen plasma, however, reduces this affinity as Mg becomes oxidized. The transitional region is formed as the resist is partially etched away by the plasma process. This process leaves behind a gradient where the level of oxidation is reduced from full to non-oxidized which nucleates ZnO growth. This hypothesis is consistent with other control experiments; oxygen plasma treated Mg doped GaN test samples, for example, did not nucleate growth under the same growth conditions. We optimized this process, and exposure to a 100 W, 100 mTorr oxygen plasma for 30 s was used to produce the illustrated structures. Nucleation in the transition region is followed by lateral epitaxial overgrowth. All growth experiments were carried out in a glass vial following a previously published procedure.⁹ In short, growth is initiated by adding zinc acetate, $\text{Zn}(\text{CH}_3\text{COO})_2$, and hexamine, $(\text{CH}_2)_6\text{N}_4$, to 70 mL of deionized water such that the solution contained 25 mM of each compound. To grow the ZnO crystals, the solution was heated in an oven to 90 °C for times ranging between 10 min to 3 h. Following the growth, samples were removed from solution and briefly rinsed with DI water. While this is the basic process, we found that the initial pH of the growth solution is an important additional parameter required for high quality crystals. It was necessary to increase the initial pH from 5.5 to 7.5 by adding small amounts of ammonium hydroxide, NH_4OH . The illustrated example used a photoresist pattern with 3 μm diameter circular openings, 6 μm center-to-center spacing, and 3 h growth time to produce the well-faceted hexagonal crystals. The largest interior dimensions of the hexagonal crystals were 4 μm , indicating that ZnO laterally

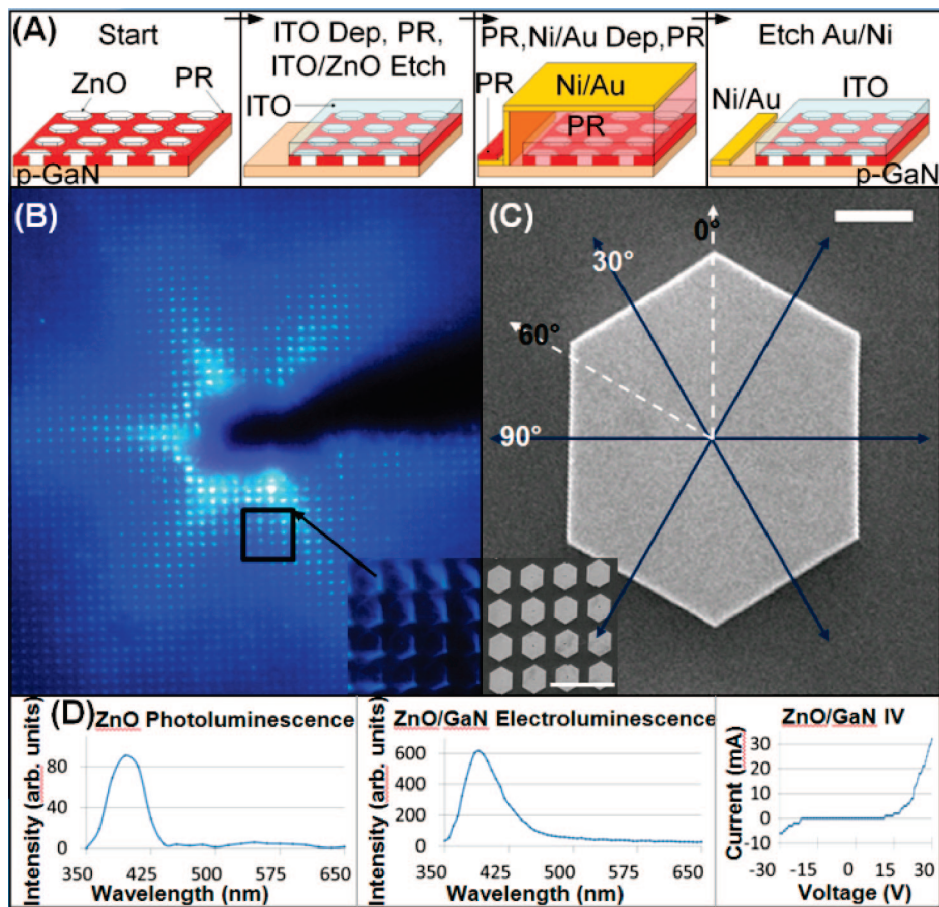


Figure 2. Fabrication and characterization of ZnO microcrystal heterojunction n-ZnO/p-GaN ultraviolet LED. (A) Processing steps. (B) Forward bias emission revealing a six-pointed star which is attributed to facet-to-facet (B inset, C inset) hexagonal propagation with reduced coupling along the 0° and 60° directions (C). (D) Photoluminescence spectrum of the ZnO, forward bias LED electroluminescence spectrum, and LED IV curve show near-band-edge emission at 3.19 eV and absence of defect peaks in the wavelength range 450–650 nm. $1 \mu\text{m}$ scale bar in C; $10 \mu\text{m}$ scale bar in C inset.

overgrew the photoresist hole by approximately $0.5 \mu\text{m}$. Lateral overgrowth occurred over the oxidized GaN as well, such that ZnO filled the photoresist holes to completely cover the GaN surface. Using the photomask, the structures can be placed with a positional accuracy (40 nm STD for $6 \mu\text{m}$ pitch = 0.7%) calculated by measuring the center-to-center distance between the ZnO crystals that have been produced. The size distribution was smaller than 1% (STD).

Inspection of Figure 1D, Figure 1F (left), and other samples shows minimal pinhole defects per area of oxygen-plasma treated ZnO crystal. Nonoxygen plasma treated control samples Figure 1E and Figure 1F (right) show significant numbers of pinhole defects and grain boundaries. More images of control samples are provided in Supporting Information. Figure S1 is a top-down SEM image of an oxygen plasma treated sample where the growth was terminated prior to completion yielding a single pinhole that is located in the center of each crystal. The control sample (Figure S2) without plasma treatment depicts randomly distributed pinhole defects and regions that resemble the morphology of a polycrystalline film. The average number of pinholes and grain boundaries is at least a factor of 10 larger for the nonplasma treated samples where the growth starts randomly in the open areas.

Figure 2 shows an array of ultraviolet heterojunction n-ZnO/p-GaN LEDs produced using the growth process to study the electro-optical properties. In short, the device was formed using the hexagonal ZnO disks that completely filled the openings in the insulating photoresist matrix. The process was more effective in eliminating pinholes and shorts between the RF sputter coated ITO top contact and GaN when compared with our earlier designs. The processing is reduced to contacting the GaN substrate using two photolithographic steps. In the first step, we used Shipley 1813 photoresist to form a $2 \text{ mm} \times 2 \text{ mm}$ sized window to the GaN using a 30 s ITO and ZnO etch in $37\% \text{ HCl}$. In the second step, we form the bottom contact which is located 1 mm away from the ITO pad using electron-beam evaporated 60 nm Ni and then 300 nm Au, photolithography, GE-6 gold and NE-9 nickel etch, and photoresist removal by rinsing with acetone, methanol, and isopropyl alcohol. This overgrowth method provides an advantage over earlier designs that required deposition of an insulating layer and polishing or etching to expose the top of the ZnO.^{2,3} The new process does not require these process steps since the ZnO crystals completely fill the openings in the insulating photoresist matrix. There are other cost advantages for solution processing of ZnO over alternative PECVD, MBE, or sputtering

methods. A potential disadvantage is that some lithography is needed. However, masks can be reused, and fabrication is effective over large area substrates.

Figure 2B shows the electroluminescence of the resulting device under forward bias, revealing a six-pointed star of violet light under a 10× optical microscope objective which cannot be explained by the layout of the array which has a square lattice. Higher resolution analysis using a 50× objective (Figure 2B inset) showed areas of high light intensity to match directions perpendicular to the hexagonal ZnO facets (Figure 2C) which suggests that some light is transmitted and coupled preferentially along directions perpendicular to ZnO facets. We have not yet changed the dimension and spacing between the ZnO microcrystal LEDs to study coupling or lasing. Figure 2D shows PL and EL spectra as recorded using a scanning monochromator and photomultiplier tube attached to the upright microscope to collect light from selected areas with a minimal spot size of 50 μm. For PL excitation, we used a hand-held ultraviolet mercury vapor lamp and 254 nm filter with a sub-350 nm cutoff, UVP, model UVGL-58. Hydrothermally grown ZnO was delaminated from the GaN substrate for ZnO photoluminescence measurement; however, EL measurements required an intact junction between n-ZnO and the p-GaN substrate. Comparison between the illustrated EL and PL spectra yields the following observation: the forward bias EL spectrum matches the PL spectrum of the ZnO crystals. The location of the PL peak near the approximately 390 nm ZnO band edge suggests that photogenerated electrons and holes do not recombine at ZnO defects in the visible. Photoluminescence of the bare GaN substrate (not shown) similarly showed a 390 nm peak and lacked defects in the visible portion of the spectrum, allowing the conclusion that both the ZnO and the GaN used here were high quality materials. Moreover, the electroluminescence spectrum (Figure 2D) shows the absence of any peaks in the 450–650 nm wavelength range, where deep-level ZnO crystal defects commonly radiate light.^{3,15} The absence of deep-level radiative defects in electroluminescence indicates that the p-GaN/n-ZnO interface generated using plasma-defined nucleation is a high quality photonic junction.

Previous work by others have shown that the defect peak wavelengths of ZnO varies widely depending on synthesis-related defect incorporation, on postprocessing treatment including exposure to gases, or annealing under various temperature. Defects common to ZnO include zinc vacancies, inclusion of hydrogen, and surface defects including pinholes and grain boundaries. Our previously reported device³ suffered from broad EL emission across the spectral range of these types of defects. The prior method used an unpatterned substrate and produced isolated nanowires that merged under continuous growth similar to those shown in Figure 1F (right) but with a slightly higher aspect ratio. Gaps/pinholes in between were filled with insulating SiO₂. The reduction of pinholes/grain boundaries and the elimination of SiO₂ filler distinguishes this paper from the previous one and is therefore believed to be the primary reason for the improved performance. It has been previously found¹² that

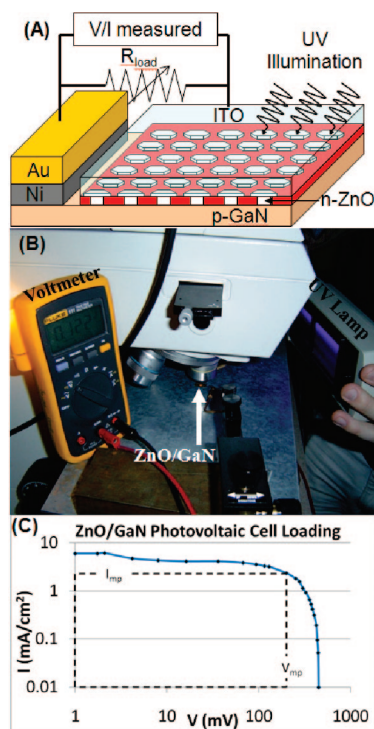


Figure 3. ZnO microcrystal UV photovoltaic cell measurement: (A) schematic, (B) photograph of the experiment, and (C) resulting IV load curve under constant illumination. The loaded device contains approximately 300 junctions with 10 μm² individual area.

dislocation defects propagated from the original crystalline template are reduced in overgrown areas. The provided explanation was that, since dislocations “cannot bend to be incorporated in the wings formed by lateral growth, the wing regions exhibit a much lower dislocation density relative to the regions of growth above the windows.” Whether or not this is the case, ZnO growth over the oxygen plasma treated area cannot be confirmed and would require similar high resolution cross-sectional TEM studies.

Illumination with a 6 W hand-held 365 nm ultraviolet lamp caused the ZnO–GaN hexagonal heterojunctions to function as a photovoltaic cell (Figure 3). The maximum open circuit voltage and short circuit junction current density was found to be 450 mV and 6 mA/cm², respectively. First order estimates yielded 1–9% electrical quantum efficiency. We do not have a precise number since the size of the active junction is presently not known with sufficient accuracy. This calculation is based on the following measurements and assumptions. The incident optical power density of the UV lamp was determined to be 3.98 mWatts/cm² as measured using an optical power meter, Anritsu, model ML9001. The optical power meter was connected to an optical power sensor, Anritsu, model MA9802A calibrated to detect a wavelength of 380 nm. The ITO formed a simultaneous contact to about 100–300 ZnO/GaN junctions which was determined from the forward bias emission picture. For an individual junction area, we used 10 μm² to represent the photoresist opening which assumes that the oxygen passivated and overgrown area does not limit transport. The junction efficiency would be larger if this assumption is

incorrect. The IV characteristic (Figure 3C) of the 300 junctions yields, $V_{mp} = 200$ mV and $I_{mp} = 70$ nA for the voltage and current at the maximum power point and fill factor of $0.17 = V_{mp}I_{mp}/V_{oc}I_{sc}$. Considering these numbers and 300 active junctions, we obtain $11\% = (200 \text{ mV} \times 70 \text{ nA})/(300 \times 10 \mu\text{m}^2 \times 3.98 \text{ mWatts/cm}^2) = \text{electrical power per optical input power}$. We performed control experiments to test if the oxygen passivated and overgrown area limits transport by comparing the recorded currents with devices that are produced with and without (old process) plasma treatment. The experiment failed to provide a conclusive answer since the old process failed to produce a pinhole free film (Figure S2) or a device without shorts. While no direct measurement is available, we do not think that the presence of an oxygen passivation significantly limits transport since the emission intensity appears uniform across individual crystals and since the calculated photovoltaic cell efficiencies would become larger than what can be anticipated for the given junction.

In summary, the reported nucleation and growth process provides a new route toward the production of ZnO micro and nanostructures at known locations (0.7% STD) with well-defined dimensions (<1% STD). The process produces high quality ZnO where deep-level radiative defects are eliminated. In addition to the demonstrated micro-LEDs and microphotovoltaic cells, we anticipate that these two features are attractive for a number of other applications that aim at integrating ZnO based devices such as ultraviolet LEDs,¹⁻³ laser cavities,¹⁶ waveguides,¹⁷⁻²⁰ high gain photodetectors,²¹ photovoltaic cells,²²⁻²⁴ sensors, piezoelectric actuators,²⁵ or micropower generators²⁶ at exact known locations on a surface. Control over location leads to the hexagonal light emission (Figure 2B) and can ultimately be used to study coupling of light and lasing. It supports the ability to individually contact single ZnO crystals and learn how light propagates from one isolated domain to another. Moreover, it may be possible to transfer single crystal domains from one substrate to another through interfacial delamination which finds applications in the field of flexible transparent electronics.

Acknowledgment. We acknowledge support of this work by NSF DMI-0556161 and NSF DMI-0621137. We also acknowledge NSF MRSEC Awards DMR-0212302, ECS-0229097, ECS-0407613 for early seed support. Correspondence and requests for materials should be addressed to H.O.J.

Supporting Information Available: Figure S1: Control sample with large dislocations, high dislocation density, high grain boundary density. Figure S2: Plasma-treated sample

with maximum pinhole density. This material is available free of charge via the Internet at <http://pubs.acs.org>.

References

- (1) Vispute, R. D.; Talyansky, V.; Choopun, S.; Sharma, R. P.; Venkatesan, T.; He, M.; Tang, X.; Halpern, J. B.; Spencer, M. G.; Li, Y. X.; Salamanca-Riba, L. G.; Iliadis, A. A.; Jones, K. A. *Appl. Phys. Lett.* **1998**, *73*, 348–350.
- (2) Wang, X.; Cole, J.; Dabiran, A. M.; Jacobs, H. O. ZnO Nanowire/p-GaN Heterojunction LEDs. *Mater. Res. Soc. Symp. Proc.* Warrendale, PA, 2007.
- (3) Wang, X.; Cole, J.; Jacobs, H. O. Electroluminescence of ZnO Nanowire/p-GaN Heterojunction Light Emitting Diodes. *Proc. 2007 NSTI Nanotechnology Conference*; Santa Clara, CA, 2007.
- (4) Alivov, Y. I.; Kalinina, E. V.; Cherenkov, A. E.; Look, D. C.; Ataev, B. M.; Omaev, A. K.; Chukichev, M. V.; Bagnall, D. M. *Appl. Phys. Lett.* **2003**, *83*, 4719–4721.
- (5) Alivov, Y. I.; Van Nostrand, J. E.; Look, D. C.; Chukichev, M. V.; Ataev, B. M. *Appl. Phys. Lett.* **2003**, *83*, 2943–2945.
- (6) Osinsky, A.; Dong, J. W.; Kausler, M. Z.; Hertog, B.; Dabiran, A. M.; Chow, P. P.; Pearton, S. J.; Lopatiuk, O.; Chernyak, L. *Appl. Phys. Lett.* **2004**, *85*, 4272–4274.
- (7) Park, W. I.; Yi, G.-C. *Adv. Mater.* **2004**, *16*, 87–90.
- (8) Jeong, M.-C.; Oh, B.-Y.; Ham, M.-H.; Myoung, J.-M. *Appl. Phys. Lett.* **2006**, *88*, 202105/202101–202105/202103.
- (9) Hsu, J. W. P.; Tian, Z. R.; Simmons, N. C.; Matzke, C. M.; Voigt, J. A.; Liu, J. *Nano Lett.* **2005**, *5*, 83–86.
- (10) Masuda, Y.; Kinoshita, N.; Sato, F.; Koumoto, K. *Crystal Growth Des.* **2006**, *6*, 75–78.
- (11) Greene, L. E.; Law, M.; Tan, D. H.; Montano, M.; Goldberger, J.; Somorjai, G.; Yang, P. *Nano Lett.* **2005**, *5*, 1231–1236.
- (12) Andeen, D.; Kim, J. H.; Lange, F. F.; Goh, G. K. L.; Tripathy, S. *Adv. Funct. Mater.* **2006**, *16*, 799–804.
- (13) Kim, J. H.; Andeen, D.; Lange, F. F. *Adv. Mater.* **2006**, *18*, 2453–2457.
- (14) Nakamura, S.; Senoh, M.; Nagahama, S.-i.; Iwasa, N.; Yamada, T.; Matsushita, T.; Kiyoku, H.; Sugimoto, Y.; Kozaki, T.; Umemoto, H.; Sano, M.; Chocho, K. *Appl. Phys. Lett.* **1998**, *72*, 211–213.
- (15) Bao, J.; Zimmler, M. A.; Capasso, F.; Wang, X.; Ren, Z. F. *Nano Lett.* **2006**, *6*, 1719–1722.
- (16) Huang, M. H.; Mao, S.; Feick, H.; Yan, H.; Wu, Y.; Kind, H.; Weber, E.; Russo, R.; Yang, P. *Science* **2001**, *292*, 1897–1899.
- (17) Yang, P.; Yan, H.; Mao, S.; Russo, R.; Johnson, J.; Saykally, R.; Morris, N.; Pham, J.; He, R.; Choi, H.-J. *Adv. Funct. Mater.* **2002**, *12*, 323–331.
- (18) Yan, H.; Johnson, J.; Law, M.; He, R.; Knutsen, K.; McKinney, J. R.; Pham, J.; Saykally, R.; Yang, P. *Adv. Mater.* **2003**, *15*, 1907–1911.
- (19) Hauschild, R.; Kalt, H. *Appl. Phys. Lett.* **2006**, *89*, 123107/123101–123107/123103.
- (20) van Vugt, L. K.; Ruehle, S.; Vanmaekelbergh, D. *Nano Lett.* **2006**, *6*, 2707–2711.
- (21) Soci, C.; Zhang, A.; Xiang, B.; Dayeh, S. A.; Aplin, D. P. R.; Park, J.; Bao, X. Y.; Lo, Y. H.; Wang, D. *Nano Lett.* **2007**, *7*, 1003–1009.
- (22) Law, M.; Greene, L. E.; Johnson, J. C.; Saykally, R.; Yang, P. *Nat. Mater.* **2005**, *4*, 455–459.
- (23) Leschkies, K. S.; Divakar, R.; Basu, J.; Enache-Pommer, E.; Boercker, J. E.; Carter, C. B.; Kortshagen Uwe, R.; Norris, D. J.; Aydil, E. S. *Nano Lett.* **2007**, *7*, 1793–1798.
- (24) Levy-Clement, C.; Tena-Zaera, R.; Ryan, M. A.; Katty, A.; Hodes, G. *Adv. Mater.* **2005**, *17*, 1512–1515.
- (25) Wang, X.; Zhou, J.; Song, J.; Liu, J.; Xu, N.; Wang, Z. L. *Nano Lett.* **2006**, *6*, 2768–2772.
- (26) Schrier, J.; Demchenko, D. O.; Wang, L.-W.; Alivisatos, A. P. *Nano Lett.* **2007**, *7*, 2377–2382.

NL0804809